JOURNAL OF GEOPHYSICAL RESEARCH, VOL. 99, NO. D11, PAGES 23,041–23,056, NOVEMBER 20, 1994

Quasi-biennial oscillation and tropical waves in total ozone

J. R. Ziemke and J. L. Stanford
Department of Physics and Astronomy, Iowa State University, Ames

Abstract. Westward and eastward propagating tropical waves in total ozone are investigated in 13 years (1979–1991) of version 6 total column ozone data from the Nimbus 7 total ozone mapping spectrometer (TOMS) satellite instrument. A clear synchronization between the stratospheric quasi-biennial oscillation (QBO) zonal winds and the fast (periods < 15 days) propagating waves in tropical TOMS data is detailed. Largest total ozone wave amplitudes (~3–6 Dobson units) occur when their phase propagation direction is primarily opposite the Singapore QBO lower-stratospheric winds. This effect is most apparent in meridionally symmetric components. Examination of specific episodes, including cross-spectral calculations with Singapore rawinsonde wind data (10–70 hPa), reveals signatures of tropically confined eastward propagating Kelvin waves of zonal wavenumbers 1-2 during the descending eastward QBO phase, consistent with acceleration of that QBO phase by Kelvin waves. The TOMS results are also consistent with possible forcing of the westward QBO wind phase by episodes of both meridionally symmetric and asymmetric westward waves (W' events in the text). However, in contrast to the case of eastward (Kelvin) waves the strongest westward events (W events in the text) appear to be filtered by, rather than forcing, the westward phase of the stratospheric QBO wind. These dominant westward episodes are interpreted as meridionally symmetric westward global normal modes and tropically confined equatorial-Rossby waves 2–6. The events exhibit phase and group speeds characteristic of wave dynamics rather than simple wind advection. These results underscore the utility of the long time series and excellent horizontal coverage of TOMS data for dynamical investigations in the relatively observation-poor tropical stratosphere.

1. Introduction

Maruyama [1991], using 29 years (January 1961 to February 1990) of upper air rawinsonde data from Singapore (and other selected tropical stations), examined annual and quasi-biennial oscillation (QBO) synchronization of tropical wave activities and the acceleration/deceleration phases of lower-stratospheric equatorial zonal winds. The absorption of eastward (westward) propagating Kelvin (Rossby-gravity) waves in the tropical lower stratosphere has been postulated to deposit eastward (westward) momentum to the atmosphere, thus contributing to the eastward (westward) acceleration of the QBO zonal winds [*Holton and Lindzen*, 1972]. However, as will be discussed below, recent modeling work suggests that serious deficiencies may occur in our understanding of the QBO, particularly with respect to forcing of the westward QBO phase.

In the Maruyama study, a distinct QBO synchronization was found between maximum Kelvin wave activities and zonal winds at pressure levels 30, 50, and 70 hPa. In contrast, Rossby-gravity (hereafter RG) waves at these pressures showed predominant annual synchronization with zonal winds; this annual variation seemed to explain the more rapid descent of the eastward (with respect to the westward) QBO winds in the lower stratosphere.

It has recently been shown that short vertical scale RG waves can be detected in total column ozone, due in part to the effects of steep vertical gradients of ozone mixing ratio in the tropical lower stratosphere. An intense tropical RG wave episode during August-September 1985 found by *Randel* [1992] in European Centre Medium Range Weather Forcast (ECMWF) wind analyses was also observed in Nimbus 7 total ozone mapping spectrometer (TOMS) data by *Stanford and Ziemke* [1993] (hereafter SZ). The simplified model used by SZ for RG waves in total ozone produced amplitudes comparable to those observed (~2–4 Dobson units (DU)), with greatest contributions originating in lower-stratospheric levels where most of the ozone and largest gradients exist. In a similar study by *Ziemke and Stanford* [1994] (hereafter ZS), the source of several episodes in tropical eastward propagating zonal waves 1–2 in TOMS total ozone were identified as lower-stratospheric Kelvin waves. In addition, the latter study found a remarkable in-phase QBO relationship between 30 hPa monthly averaged westward zonal winds from Singapore (1°N, 104°E) and fast eastward propagating tropical zonal waves 1–2 in TOMS data.

Until recently, few studies have focused specifically on tropical TOMS data. In one of these, *Shiotani* [1992]

Paper number 94JD02149.
0148-0227/94/94JD-02149$05.00

investigated long-term variability in TOMS data, primarily for the zonal mean and wave 1. The present study examines relationships between QBO zonal winds and relatively fast (periods of around 15 days and less) zonally propagating tropical waves 1–6 in TOMS ozone. This investigation expands the work of SZ and ZS, comparing eastward and westward equatorial wave pulses with respect to vertical descent and variation of QBO westward and eastward wind phases.

SZ observed RG waves in TOMS but showed only one case and made no reference to QBO variability in tropical TOMS ozone waves. A major component in the present paper is detailing QBO variability of wave activity in TOMS westward waves 3-6, which neither SZ nor ZS did. This paper provides further insight about the types of waves contributing to the westward TOMS features; the westward waves are suggested to be primarily RG waves, long vertical wavelength equatorial-Rossby (hereafter ER) waves and global normal modes.

One of the main points of ZS was to identify a QBO variability in tropical TOMS eastward waves 1-2, in which it was shown that largest wave amplitudes (typically 3–5 DU) in equatorial total ozone occurred roughly 180°out of phase with respect to 30-hPa Singapore winds. Included in the present study of eastward waves 1-2 are integrated spectra and cross-spectra calculations with zonal winds. This analysis uses cross-spectra calculations to derive QBO meridional amplitude structures of total ozone/wind phases. Tropical TOMS analyses show fast (periods < 15 days) eastward waves 1-2 QBO synchronization peaking near the equator, at times of maximum eastward acceleration of zonal winds, in contrast to westward waves 3-6 which peak in the tropics around latitudes 10°-15°(relative minimum at the equator). In overall perspective, QBO cross-spectra calculations suggest Kelvin waves in eastward waves 1-2 and primarily mixed ER and global normal modes in westward waves 3-6 (different wind/wave relationships are observed for eastward waves 1-2 and westward waves 3-6). SZ and ZS did not detail meridional structures or wind/wave phases on QBO timescales.

Meridionally asymmetric waves 3–6 in TOMS, conceivably including RG waves, are found to exhibit relative maximum amplitudes around times of westward acceleration of the QBO zonal winds. The present paper also compares strongest events in meridionally symmetric westward waves 2-6 TOMS with geopotential heights, identifying ER and global normal modes as the most probable wave types.

2. Data and Analyses

The TOMS data examined in this study were obtained by regridding 1.25°longitude × 1°latitude CD-ROM data provided by Goddard Space Flight Center (GSFC). Details of the TOMS instrument and our data regridding are given in SZ. This regridding yielded 5° × 5°daily fields extending from longitudes 180° to 175°E and latitudes 85°S to 85°N. Only latitudes 30°S to 30°N were used in this study except for a few select cases (e.g., cases involving global normal modes). Space-time spectra were computed with time series averages removed and a 10%–10% cosine taper window applied to reduce leakage. Power spectra for 1979–1991 used a 180-day window length stepped forward in time at 1-month intervals. Power spectra calculations involved a decomposition in space-time variables into eastward and westward components (see, for example, the appendix of *Ziemke and Stanford* [1990]). Raw power ordinates are defined in this study by $(2\Delta f)^{-1}[A^2(k,\omega) + B^2(k,\omega)]$, where Δf is the unit bandwidth (1 day^{-1} here). $A(k,\omega)$ and $B(k,\omega)$ were calculated using a fast Fourier transform (FFT) in both time and space from the following zonal space-time harmonic definition for total column ozone Ω:

$$\Omega_{\pm}(x,t) = \sum_{k=0}^{\pi/\Delta x} \sum_{\omega=0}^{\pi/\Delta t} \Big[A_{\pm}(k,\omega)\cos(kx \pm \omega t) + B_{\pm}(k,\omega)\sin(kx \pm \omega t) \Big]. \quad (1)$$

Variable t (x) denotes time (zonal distance), Δt (Δx) is the temporal (spatial) sampling interval, k is the zonal wavevector, ω is the angular frequency, and + (−) denotes the westward (eastward) propagating component of $\Omega(x,t)$.

A 0.25–0.5–0.25 running mean "smoothed spectral estimator" was applied once to raw power ordinates to estimate power spectra. Spectral power involving more than one zonal wavenumber were calculated by adding together power spectral values from each individual wavenumber. Spectral amplitude, used in several plots in this study, is the square root of twice the smoothed spectral power.

For this study, 12 years (January 1, 1980 to December 31, 1991) of daily geopotential heights from the British Meteorological Office (hereafter BMO) were used in conjunction with the TOMS data. The BMO data sets extend from the lower troposphere up to the stratopause on the following 11 pressure surfaces: 850, 500, 300, 200, 100, 50, 20, 10, 5, 2, and 1 hPa. Up to 100 hPa the grids are NMC analyses; satellite radiances are used to obtain stratospheric levels. Horizontal gridding is the same 5°×5° mesh constructed for TOMS.

The zero phase shift band-pass filter response function given by *Murakami* [1979] was applied in frequency space (using an inverse FFT) to reconstruct band-pass filtered time series. Tabulated monthly mean zonal winds from Singapore (B. Naujokat, Free University of Berlin, personal communication, 1992) for years 1979-1991 at pressure levels 70, 50, 40, 30, 20, 15, and 10 hPa were used in this study to provide a clear QBO wind index upon which TOMS tropical spectra are compared. Other rawinsonde station data were not employed in this study since the main focus of this investigation is synchronization between fast tropical waves in TOMS and the QBO signal in equatorial zonal winds; the QBO, of long period (~26–32 months) is mostly zonally symmetric, so that use of the single station at Singapore is anticipated to provide an adequate QBO wind proxy.

3. Theory of Total Ozone Perturbations Induced by Atmospheric Wave Modes

In our earlier TOMS tropical wave papers, SZ and ZS, episodes of RG and Kelvin waves were identified in TOMS total ozone data. How such perturbations can be induced by atmospheric wave motions is discussed next, in some detail for the simpler case of Kelvin waves (possessing no meridional velocity) and more schematically for the more general cases of other equatorial waves.

The pressure integration expression for total column ozone (Ω) is given by integrating volume mixing ratio (X) over pressure (P) from zero pressure (infinite altitude) to pressure P_S (Earth surface): $\Omega = A \cdot \int_0^{P_S} dP\, X$, where A is a constant ensuring units DU in the integration (A=7880 DU Pa^{-1}).

In a derivation similar to that given by *Andrews et al.* [1987] using Cartesian coordinates (p. 354), it can be shown that a similar flux form of the tracer continuity equation in spherical pressure coordinates is given by

$$\frac{\partial X}{\partial t} + (a\cos\phi)^{-1}\left[\frac{\partial(uX)}{\partial\lambda} + \frac{\partial(vX\cos\phi)}{\partial\phi}\right] + \frac{\partial(\omega X)}{\partial P} = S \tag{2}$$

where ω is the total time derivative of pressure, a is the Earth's radius, S is a net sink/source, and λ and ϕ are longitude and latitude, respectively. All other symbols are standard. Applying the pressure integration expression of total ozone to the left-hand and right-hand sides of (2) results (with boundary condition $X(P=0)=0$)in the following flux form for total ozone time tendency ($\frac{\partial\Omega}{\partial t}$):

$$\frac{\partial\Omega}{\partial t} = -(a\cos\phi)^{-1}\left[\frac{\partial F_u}{\partial\lambda} + \frac{\partial(F_v\cos\phi)}{\partial\phi}\right] - A\cdot\omega(P_S)X(P_S) + A\cdot\int_0^{P_S} dP\, S. \tag{3}$$

In (3), $F_u = A\cdot\int_0^{P_S} dP\, uX$ and $F_v = A\cdot\int_0^{P_S} dP\, vX$ denote pressure integrated zonal and meridional fluxes of ozone. As noted by *Bowman* [1990], a good approximation is to drop the second to last term on the right-hand side of (3), and for waves with periods ~1 week (similar to this study), another good approximation is to drop the last term on the right-hand side. The zonal mean (written with overbar) and zonally asymmetric part (denoted by prime) of (3) yield

$$\frac{\partial\overline{\Omega}}{\partial t} = -(a\cos\phi)^{-1}\left[\frac{\partial(\overline{F}_v\cos\phi)}{\partial\phi}\right] \tag{4a}$$

$$\frac{\partial\Omega'}{\partial t} = -(a\cos\phi)^{-1}\left[\frac{\partial F_u'}{\partial\lambda} + \frac{\partial(F_v'\cos\phi)}{\partial\phi}\right]. \tag{4b}$$

For small-amplitude tropical Kelvin, ER and RG waves, a reasonable approximation is to linearize terms in (4b) about zonal means $\overline{u}$ and $\overline{X}$. Assuming that $|u'| \ll |\overline{u}|$, $X' \ll \overline{X}$ and $|v'| \sim |\overline{v}| \sim |u'|$, then to first order in deviations it follows that

$$\frac{\partial F_u'}{\partial\lambda} = A\cdot\int_0^{P_S} dP\left[\frac{\partial u'}{\partial\lambda}\overline{X} + \overline{u}\frac{\partial X'}{\partial\lambda}\right] \tag{5a}$$

$$\frac{\partial F_v'}{\partial\phi} = A\cdot\int_0^{P_S} dP\,\frac{\partial v'}{\partial\phi}\overline{X}. \tag{5b}$$

3.1. Total Ozone Perturbations Induced by Kelvin Waves

Examination of (4b) above indicates that tropical Kelvin (and also ER and RG) wave perturbations in total ozone are due to pressure-integrated horizontal wind fluxes of ozone. But in the tropical lower stratosphere, vertical gradients of ozone can be very strong and must surely have an impact on the detectability of tropical waves in TOMS. Expression (4b) does not appear at first to have any relation to vertical gradients of ozone.

In the simplest case, that of pure Kelvin waves with no meridional motions, F_v' is zero. For Kelvin wave perturbations the mass continuity equation is given by $\frac{\partial u'}{\partial\lambda} = -a\cos\phi\cdot\frac{\partial\omega'}{\partial P}$, from which it follows that $\frac{\partial u'}{\partial\lambda}\overline{X} = a\cos\phi\cdot[\omega'\frac{\partial\overline{X}}{\partial P} - \frac{\partial(\omega'\overline{X})}{\partial P}]$. This latter expression is substituted into (5a), followed by pressure integration with boundary conditions $\omega'(P_S) = 0$ and $\overline{X}(P=0) = 0$. The expression for Kelvin wave perturbations in total ozone time tendency then becomes

$$\frac{\partial\Omega'}{\partial t} = -A\cdot\left[\int_{P_1}^{P_2} dP\,\overline{u}\frac{\partial X'}{\partial x} + \int_{P_1}^{P_2} dP\,\omega'\frac{\partial\overline{X}}{\partial P}\right]. \tag{6}$$

In (6), x is standard zonal (eastward) distance ($\frac{\partial}{\partial x} = (a\cos\phi)^{-1}\frac{\partial}{\partial\lambda}$). P_1 and P_2 ($P_1 < P_2$) denote minimum and maximum pressure integration levels, outside of which Kelvin wave perturbations are taken to be zero due to absorption. The first term on the right-hand side of (6) represents a zonal mean wind effect, while the last term shows an important coupling of ω' with the vertical pressure gradient of zonal mean ozone. This latter term, as shown by ZS, may be large in the tropical lower stratosphere where most ozone and largest vertical gradients exist.

For ER and RG waves there is an additional meridional wind component which Kelvin waves do not have. For simplicity, we will now discuss signatures of ER and RG waves in total ozone using a schematic diagram approach.

3.2. Meridional Symmetries of Rossby-Gravity and Equatorial-Rossby Modes

One of the primary concerns in the present study is to identify the types of fast tropical wave events observed in TOMS data. For eastward waves with periods shorter than ~15 days, ZS identified several episodes of Kelvin waves in TOMS. In the present study we attempt to identify the types of waves observed in westward propagating tropical waves 2–6. Here we will examine signatures of two types of waves which are likely candidates: ER and RG waves.

Perturbation signatures in ozone caused by these tropical waves will depend upon the background gra-

dient field in lower-stratospheric ozone mixing ratio. Figure 1 shows a simplified schematic diagram outlining symmetry forcing effects on tropical ozone caused by the horizontal and vertical wind fields from lower-stratospheric westward propagating linear ER and RG waves. The meridionally symmetric background ozone mixing ratio field shown corresponds to equinox conditions. During solstice, there is ~10°–15° latitudinal shift of this distribution into the summer hemisphere, but general conclusions based on Figure 1 will be qualitatively similar. Near solstice this shift might have an important impact in changing the detected meridional symmetry of tropical ozone waves, particularly RG waves, which according to the simplified model by SZ showed largest amplitudes occurring only ~5°–10°from the equator.

For linear equatorial beta-plane wave modes [cf. *Andrews et al.*, 1987], it can be shown that the meridional velocity for ER modes is dependent on latitude through $H_n(\eta)$, while the vertical velocity's latitude dependence comes through a linear combination of the functions $H_{n+1}(\eta)$ and $H_{n-1}(\eta)$. Here, $H_n(\eta)$ denotes an nth order Hermite polynomial function of variable η (η is equivalently latitude, multiplied by a constant). The first three Hermite polynomials are given by $H_0(\eta) = 1$, $H_1(\eta) = 2\eta$, and $H_2(\eta) = 4\eta^2 - 2$. Consecutive Hermite polynomials have opposite odd/even function signatures in η. For the background ozone distribution shown in Figure 1, linear ER modes with $n = 1, 3, 5, ...$, would induce meridionally symmetric ozone perturbations (Figure 1a), whereas ER modes with $n = 2, 4, 6, ...$, and RG waves ($n = 0$) will be expected to exhibit antisymmetric ozone signatures (Figure 1b).

Summarizing, waves in total ozone, induced by dynamical tropical waves, have structures that depend on both the mean background ozone gradients and the detailed nature of the particular forcing wave. Perturbations in TOMS total column ozone caused by ER and/or RG waves correspond to vertical summations of perturbations induced at various altitudes by these waves. Figure 1 shows schematically how different contributions to total column are induced at different altitudes. Depending on the signs of the background ozone gradients and local perturbation wind component, different terms in the tracer continuity equation contribute either positively or negatively, adding to, or partially canceling one another in the total column vertical summation. (Note that meridional perturbation winds induce opposite effects at altitudes above and below ~30 hPa.)

It should also be mentioned in reference to the comparably small amplitudes observed (~1–3% total column) in this study that there are biasing effects internal to TOMS measurements due to clouds. This is because when clouds are present, TOMS version 6 retrieval algorithms must estimate, using climatological cloud heights, the ozone that lies below the clouds. The study by *Thompson et al.* [1993] showed that corrections to TOMS associated with low (~700–900 hPa) marine stratocumulus clouds west of Africa during August-October 1989 were as much as ~-20 and -5 DU for daily and monthly means, respectively. These corrections to

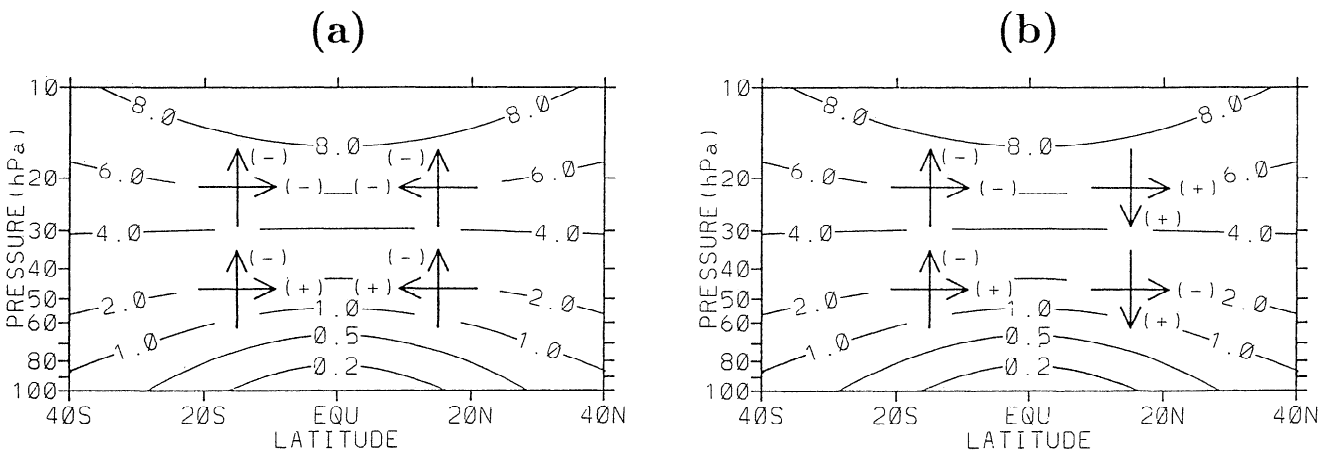

Figure 1. Schematic illustration of how lower-stratospheric meridional and vertical wind perturbations from meridionally (a) symmetric and (b) antisymmetric modes induce ozone mixing ratio changes according to the tracer continuity equation $X_t + uX_x + vX_y + wX_z = S$, where X is volume mixing ratio (lines of constant, zonally averaged X are labeled by 0.2 to 8.0 parts per million), v and w are meridional and vertical winds, and subscripts denote partial differentiation. The source/sink term S can be taken to be zero for the altitude region shown in this figure. (a) Equatorial-Rossby (ER) ($n = 1, 3, 5, ...$) modes couple with the background ozone field (shown here at equinox), resulting in symmetric perturbations in ozone. Pluses and minuses denote corresponding signs of ozone perturbations caused by the indicated wind component (vertical and meridional wind directions given by arrows). Zonal/temporal phase differences between vertical and meridional winds depend on the specific type of wave and are not indicated. Note that meridional wind (v) advection induces opposite effects in ozone perturbations at altitudes above and below ~30 hPa. (b) Same as Figure 1a but for meridionally antisymmetric ER ($n = 2, 4, 6, ...$) modes and RG waves.

TOMS relate to extreme cases of cloud biases and in comparison to the fast propagating waves investigated in this study are stationary in nature. It is beyond the scope of this paper to determine the precise role of clouds in the many events of fast propagating tropical disturbances examined. Rather, it is likely that variabilities in ozone provide the primary source for these fast TOMS events. The simplified RG and Kelvin wave models by SZ and ZS showed that dynamical forcing of ozone can itself provide amplitudes comparable to those observed (~2–5 DU).

4. Observation of Quasi-Biennial Oscillation (QBO) Synchronization

4.1. Meridionally Symmetric Waves and 30-hPa QBO Winds

Power spectra for meridionally symmetric eastward zonal waves 1–2 and westward waves 3–6 are shown in Figure 2. To highlight known meridional characteristics of Kelvin waves and westward waves of many sorts, eastward waves 1–2 (westward waves 3–6) spectra in this figure were constructed for meridionally symmetric waves by averaging time series between latitudes 5°N, equator, and 5°S (15°N and 15°S). The most distinct feature observed is a clear out-of-phase relationship between 30-hPa QBO zonal winds and wave activities of both westward and eastward components. The 30-hPa winds were chosen among all Singapore levels to emphasize this unique out-of-phase behavior in the lower stratosphere.

Special wave events (E1–E5 and W1–W5, with or without primes) marked in Figure 2 will be examined in greater detail in later sections. For the present these marked episodes denote broad windows in time (~1/2 year), but in later sections they will be represented by shorter time segments centered about specific events.

The westward events W1–W5 in Figure 2 appear to have little or no connection to the westward accelera-

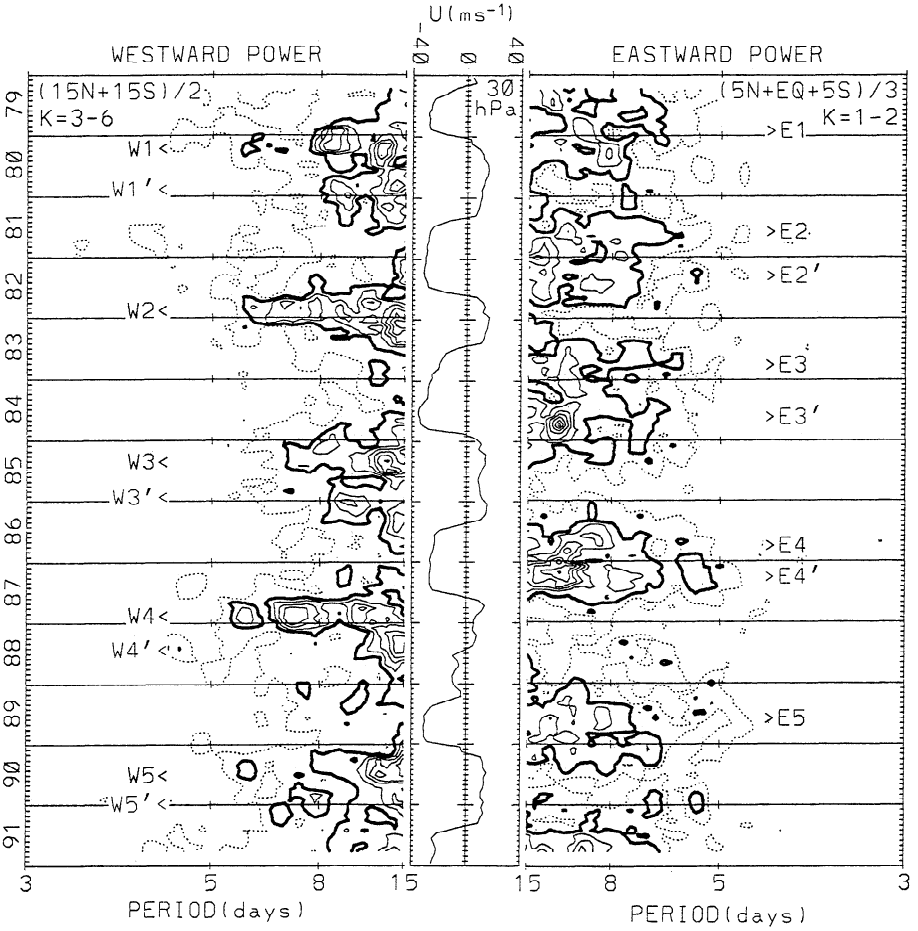

Figure 2. Calculated meridionally symmetric westward/eastward total ozone mapping spectrometer (TOMS) power spectra (units DU^2 day) covering 1979-1991 for westward propagating zonal waves 3–6 (left) and eastward propagating zonal waves 1–2 (right). Monthly mean 30-hPa zonal winds (units ms^{-1}) from Singapore are shown in middle. Symmetric westward waves 3–6 (eastward waves 1–2) spectra are computed from time series averaged between 15°N and 15°S (5°N, equator, and 5°S). A 180-day window was stepped forward in time at 1-month intervals to compute spectra. Only largest frequencies shown, with periods in days indicated (15, 8, 5, and 3 days). Solid (dashed) contours for waves 1–2 are 0.02,0.04, ... (0.01), with 0.02 darkest; solid (dashed) contours for waves 3–6 are 0.06,0.09, ... (0.03), with 0.06 darkest. Symbols E1–E5 and W1–W5 (with or without primes) identify specific 60-day case episodes (see text).

tion phase of the 30-hPa QBO winds shown, as they are seen to occur around times of eastward rather than westward wind acceleration. However, events W1′ and W3′–W5′ do exist during times of westward acceleration. All of these westward events will be discussed in following sections.

E2, E3′ and E4′ in Figure 2 are three eastward propagating episodes in TOMS data investigated previously by ZS. In that study it was shown that these three cases were consistent with lower-stratospheric slow (periods ~5–15 days) Kelvin waves. Using 15 years (1974-1988) of 10 to 70-hPa Singapore winds and temperatures, *Shiotani and Horinouchi* [1993] found that largest zonal wind power spectra (integrated periods 8.3–30.3 days, attributed to Kelvin wave activity) occurred during the transition from westward to eastward QBO winds. Note that in Figure 2, around 1–4 months prior to times of maximum eastward acceleration of the 30-hPa QBO winds, eastward traveling waves 1–2 exhibit large amplitudes, particularly for episodes E3′ and E4′. These two episodes, as discussed by ZS, coincide with two apparent Kelvin wave events shown by Shiotani and Horinouchi; upon comparing the peak zonal wind spectra at different pressure levels shown in their Figure 3 with E3′ and E4′ in our Figure 2, it can be deduced that these Kelvin wave perturbations in ozone appear localized to pressure levels ~30–70 hPa. Shiotani and Horinouchi also found Kelvin wave activity during the descending eastward QBO wind phase in late 1979 to early 1980. Eastward waves 1–2 event E1 in Figure 2 also shows evidence of enhanced wave activity at this time; this episode and several others will be examined next.

4.2. Tropical Episodes and Vertical Distribution of QBO Winds

A more detailed investigation of this synchronization phenomenon is provided in Figure 3 which shows Singapore 10–70 hPa monthly zonal winds (top) and selective waves 1–6 monthly spectra (bottom). Clear QBO synchronization is again evident in both meridionally symmetric waves 1–2 and 3–6 (dark and light solid curves) and also for antisymmetric waves 3–6 (dashed) spectra.

All of the eastward events E1–E5 and E2′–E4′ shown in Figure 3 occur during predominant westward winds throughout most of the wind levels shown, with events E1, E2′–E4′, and E5 occurring precisely during the descending eastward transition phase of the QBO zonal winds at altitudes above the 30-hPa pressure level. As discussed by ZS, these episodes are probably Kelvin waves in total ozone.

Westward events W1′ and W2–W5 in Figure 3 all occur during predominant eastward Singapore winds with

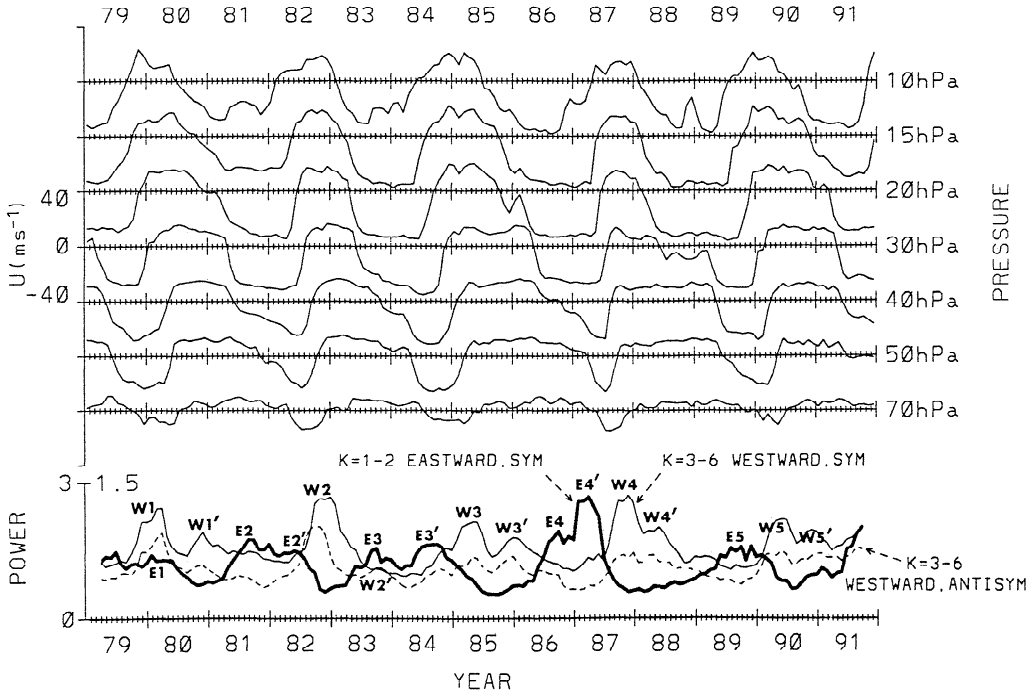

Figure 3. (Top) Monthly mean 10 to 70-hPa zonal winds (units ms^{-1}) from Singapore (1°N, 104°E) plotted for 1979–1991. Spectra calculations use 180-day window stepped forward in time at 1-month intervals (same as Figure 2). (Bottom) Power spectral density summed over frequency (2- to 15-day periods) for meridionally symmetric eastward waves 1–2 (dark solid), meridionally symmetric westward waves 3–6 (light solid), and meridionally asymmetric westward waves 3–6 (dashed). Symmetry of eastward waves 1–2 spectra formed by averaging integration results among latitudes 5°S, equator, and 5°N. Symmetric (antisymmetric) waves 3–6 power spectra formed by spectral analysis of $[T(15°\ N)+T(15°\ S)]/2$ ($[T(15°\ N)-T(15°\ S)]/2$) where T denotes a TOMS time series. Units are DU^2. Events E1–E5 and W1–W5 (with or without primes) are discussed in text.

corresponding wind speeds ~10–20 ms^{-1} throughout most of the pressure levels shown. Episodes W2–W5 occur at identical phases of these winds, that is, during the descending eastward transition phase of the QBO winds around 50–70 hPa. (The zero wind altitude is higher, near 20 hPa for event W1′.) Event W1 in Figure 3 coincides with strong westward Singapore winds at 40 and 50 hPa, so that W1 (both meridionally symmetric and antisymmetric components) could be caused by simple westward wind advection of ozone anomalies. It should be noted that Singapore winds near the equator are still a fair indicator of the direction of zonal winds for westward events in these tropical latitudes, due to dominance of lower-stratospheric tropical QBO zonal winds which have largest values along the equator and latitudinal e-folding decay latitude ~15° in both hemispheres.

Events W1′–W5′ in waves 3–6 symmetric components (light solid) in Figure 3 appear to be of reduced magnitude compared to their counterpart episodes W1–W5 six to eight months earlier (W2′ in fact shows no relative peak for symmetric waves 3–6). One possibility is that the descending QBO westward winds in the upper altitudes shown may have a filtering (critical level absorption) effect on W1′–W5′. If simple westward wind advection were the major cause of all of these westward episodes, it is difficult to explain why westward episodes W1′–W5′ would have smaller amplitudes than their counterpart episodes W1–W5, unless significant absorption is occurring for W1′–W5′. Absorption of meridionally symmetric and asymmetric waves 3–6 during events W1′–W5′ could in principle contribute to the westward acceleration phase of the QBO zonal winds. According to the theoretical study by *Andrews and McIntyre* [1976], such low frequency planetary-scale westward waves can contribute to the westward acceleration of the tropical zonal mean flow.

As shown by SZ, RG waves are detectable in TOMS ozone despite the fact that these waves generally have short vertical wavelengths, typically ~5 km. It is likely that during the westward transition phase of the QBO winds, RG waves propagate upward and are absorbed as they approach a critical level in the strong westward winds above. Their detectability in TOMS ozone depends upon large ozone gradients in tropical lower-stratospheric ozone. In TOMS ozone, RG wave signatures may generally be meridionally asymmetric (see section 3). In such a case, the meridionally asymmetric waves 3–6 (dashed curve) in Figure 3 should include contributions from RG waves during the westward transition phase of the QBO. Indeed, meridionally asymmetric waves 3–6 for events W1′–W5′ in Figure 3, coinciding with the westward acceleration phase of the QBO, do show evidence of relative maxima in each case. (One of these, W3′, is just a few months after the August–September 1985 mixed waves 5–6 RG episode examined by SZ.)

We summarize these results by first saying that the largest pulses of equatorial waves (both eastward and westward propagating) observed in TOMS data propagate primarily opposite in direction to lower-stratospheric winds, thus generally ruling out simple wind advection effects. This behavior is broadly consistent with simple predictions from wave dynamics in which strong wave absorption is predicted for a vertically propagating wave approaching a critical level where its zonal phase velocity equals, in both magnitude and direction, the background zonal wind. No critical level exists if these velocities are in opposite directions, and the wave may continue to propagate upward into the stratosphere from source regions below [cf. *Andrews et al.*, 1987]. Eastward waves 1–2 events in TOMS, including Kelvin wave response in total ozone, show significant amplitudes (e.g., see events E2′–E4′ and E5) during the eastward transition phase of the QBO winds in the upper levels shown in Figure 3. Meridionally asymmetric waves 3–6 in TOMS (conceivably including RG waves) show enhanced wave activity during the westward transition phase of the QBO zonal winds, implying a possible role in the westward wind acceleration. In addition, symmetric waves 3–6 show evidence of wave absorption during this transition phase, implying perhaps some involvement in the westward acceleration phase of the QBO winds. (Meridionally asymmetric waves 3–6 also show this: compare W1 with W1′ and W2 with W2′.)

5. Eastward Component Studies

5.1. Mean QBO Synchronization

Figure 4a shows selective integrations of monthly TOMS power spectra over wavenumber (eastward waves 1–2) and frequency (periods < 15 days), evaluated at latitudes 20°S–20°N. Each spectral series in this figure includes combined meridionally symmetric and antisymmetric components. To provide amplitude comparisons between spectra at different latitudes, each spectral series in Figure 4a was rescaled by dividing each spectral value by the corresponding maximum series amplitude. Numbers in parentheses denote these maximum amplitudes, relative to equatorial eastward waves 1–2 (value 1.0 shown in figure). These calculations use monthly spectral series centered on April 1979 through March 1991, with all monthly spectra following March 1991 rejected due to anomalously large amplitudes. (Beginning mid-June 1991, there is aerosol contamination from the Mount Pinatubo eruption.) Figure 4a indicates an obvious QBO (2–3 year) variability at low latitudes (centered about the equator): the clear annual variation seen at 20° latitudes is replaced in lower latitudes by perturbations with QBO timescales.

The apparent QBO synchronization between tropical zonal winds and tropical TOMS waves 1–2 is examined further using calculated QBO cross spectra between zonal winds from Singapore and TOMS spectral series from Figure 4a. QBO cospectra and quadspectra between these two data sets are shown in Figure 4b. Although the same spectral series in Figure 4a are used, each eastward waves 1–2 series was prenormalized to peak value 1.0 (see Figure 4 caption).

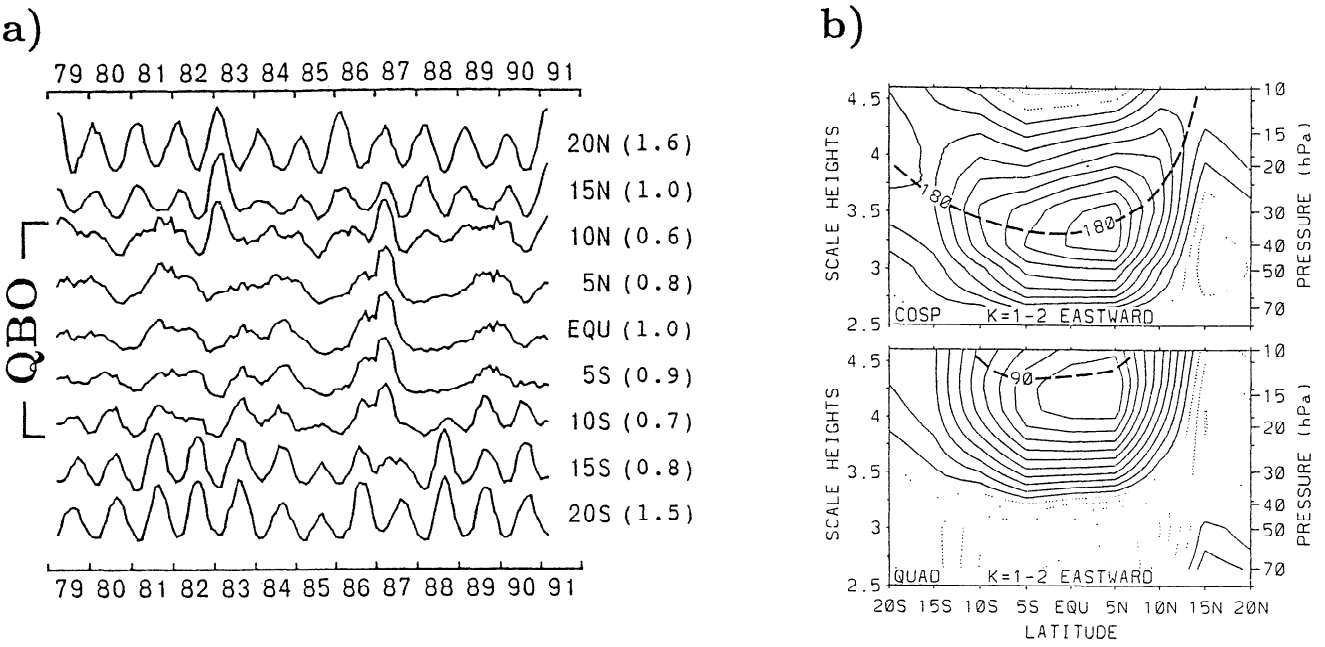

Figure 4. (a) Latitude versus time spectral series integrations (summations) over wavenumber and frequency (periods < 15 days). Series shown are for eastward propagating waves 1–2. Calculations use 180-day window stepped forward in time at 1-month intervals (uses same waves 1–2 series from Figure 3). Numbers in parentheses denote maximum power series values relative to the equatorial eastward waves 1–2 series (denoted 1.0). Units, none. (b) Log-pressure scale height versus latitude plots of quasi-biennial oscillation (QBO) (spectrally integrated over QBO periods) cospectra (top) and quadspectra (bottom) calculated between Singapore monthly zonal winds (10–70 hPa) and spectrally integrated normalized monthly power series (see section 5.1). Units, ms^{-1}. With 144 consecutive monthly spectral estimates, QBO cospectra and quadspectra estimates involved smoothing cross power for frequency indices p=4,5,6 (frequency ($month^{-1}$) is given by $p/144$). (Top) Cospectra between eastward waves 1–2 and Singapore westward zonal winds. Dashed (solid) contours begin at -0.002 (zero) in decrement (increment) by 0.002. Dark dashed curves denote phase lead (in degrees) of eastward waves 1–2 relative to westward zonal winds. (Bottom) Quadspectra, with same contouring and phase notation of cospectra.

Eastward waves 1–2 in Figure 4b exhibit largest QBO cospectra (top frame) when their direction of propagation is essentially opposite the Singapore zonal winds (~180°phase shifts indicated in figure). This observation is consistent with basic dynamical principles whereby, in the absence of other effects, such propagating waves are expected to have largest amplitudes in the absence of critical levels (noted in section 4.2).

Kelvin waves appear responsible for the cospectra maxima near the equator around pressure levels 30–40 hPa in Figure 4b (top). Further calculations of QBO quadspectra for eastward waves 1–2 in Figure 4b (bottom frame) reveal a one-quarter QBO cycle phase lead of TOMS spectra relative to eastward Singapore zonal winds near 15 hPa, indicating that maximum eastward waves 1–2 coincide with maximum eastward acceleration of the QBO zonal wind around 15 hPa. (Because the quadspectrum (Figure 4b) is zero near 35 hPa, this indicates that TOMS and Singapore winds are either exactly in or out of phase at this level, and Figure 4a reveals them to be 180°out of phase. This generalized 13-year result is also observed in the case examples E1, E2′–E4′, and E5 in Figure 3.) These results are consistent with a downward propagation of Kelvin wave absorption beginning in the top levels of Figure 4b and with the concept of absorption of Kelvin waves contributing to the eastward acceleration phase of the equatorial QBO zonal winds.

5.2. Examples of Kelvin Waves in Total Ozone

Kelvin wave signatures in total ozone for events E1, E3, and E5 are shown in Figure 5. These three cases are not the same as those shown by ZS. Kelvin wave features observed in the lowest latitudes in Figure 5a are equatorial confinement of eastward components and a dominant wave 1 in which periods are ~8–10 days. These features are characteristic of slow Kelvin waves in the lower stratosphere. Larger power amplitudes in Figure 5a observed at extratropical latitudes in both hemispheres arise from disturbances in TOMS that are predominantly eastward propagating outside the tropics due to effects from the tropospheric eastward zonal wind jets. Hovmöller diagrams in Figure 5b, band-pass filtered to capture responses shown in Figure 5a, include both eastward and westward phase components. Maximum amplitudes are ~3–5 DU with temporally changing eastward phase periods ~6–12 days.

Events E1, E3, and E5 are not caused by simple eastward wind advection of ozone. To produce wave 1 eastward periods of 8 to 10 days from advection, it would

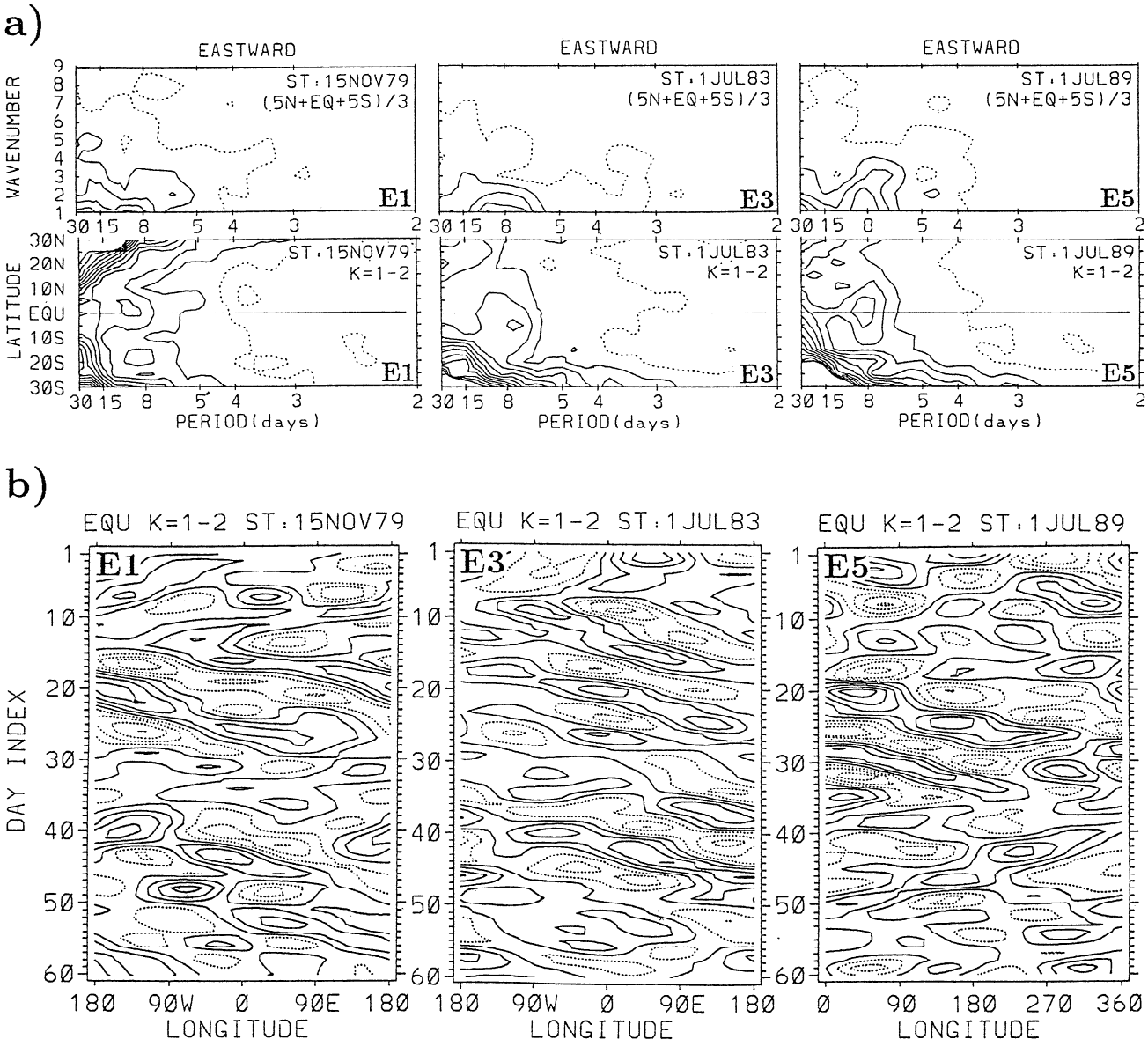

Figure 5. Kelvin wave events E1, E3, and E5. Data set lengths: 60 days with starting dates indicated. (a) (top) Eastward component spectral amplitudes (units DU) plotted as zonal wavenumber versus frequency (periods in days shown); dashed (solid) contours are 0.1 (0.2,0.3,...). (Bottom) Eastward spectral amplitudes (DU) for combined waves 1–2, plotted as latitude versus frequency; dashed (solid) contours are 0.15 (0.3,0.45,...). (b) Hovmöller (time versus longitude) diagrams of zonal waves 1–2 band-pass filtered episodes E1, E3, and E5 total ozone (DU). Eastward and westward components combined. Band-pass frequency response for all episodes: half amplitude at 20 and 3-day periods. Dashed (solid) contours begin at -1 (zero) and decrement (increment) by 1.

require eastward winds of 58 and 46 ms^{-1}, respectively. But for all of these three events combined, the largest monthly mean Singapore eastward wind between 10 and 70 hPa was found to be 24 ms^{-1}, too small to account for the phenomena by simple advection effects.

6. Westward Component Studies

6.1. Mean QBO Synchronization

Figure 6a shows selective integrations of monthly TOMS power spectra over wavenumber (westward waves 3–6) and frequency (periods < 15 days), evaluated from 20°S to 20°N. At each latitude, westward waves 3–6 series values were divided by the corresponding maximum series value calculated in eastward waves 1–2 series. Numbers in parentheses denote these maximum amplitudes, relative to equatorial eastward waves 1–2 (value 1.0 shown earlier in Figure 4a).

Significant amplitudes in SH westward waves 3–6 spectra during the two El Niño–Southern Oscillation (ENSO) events in 1982–1983 and 1987 are evident in Figure 6a. These two ENSO events, corresponding to episodes W2 and W4 in Figures 2 and 3, coincide with

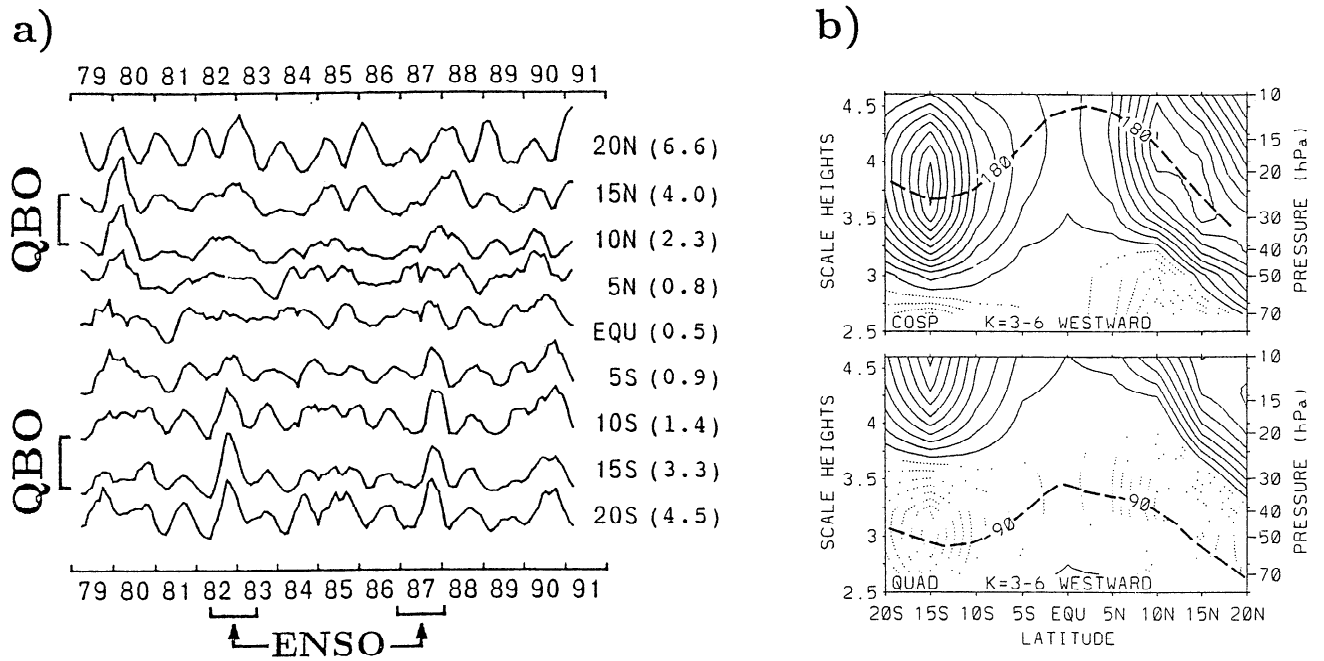

Figure 6. Same as Figure 4 but instead for westward waves 3–6 and eastward zonal winds. (a) Numbers in parentheses again denote maximum power series value relative to equatorial eastward waves 1–2 series (denoted 1.0 in Figure 4a). (b) Contour values are those from Figure 4b but multiplied by 3. Dark dashed curves denote phase lead of westward waves 3–6 relative to eastward zonal winds.

enhanced wave 2 activity (discussed below in section 6.2). Conceivably, the two southern hemisphere (SH) maxima in westward waves 3–6 may be related to localized ENSO-enhanced normal modes or mixed westward propagating ER or RG modes during favorable eastward QBO tropical zonal winds (see Figure 3). Note that the major eruption of El Chichon in April 1982 injected a large mass of aerosols into the stratosphere, but due to a lack of tropical eddy mixing in the following weeks the particles remained in the northern hemisphere (NH) at latitudes around 0°–30°N [*McCormick and Osborn*, 1985.] In contrast, anomalous spectral amplitudes in TOMS data during 1982 shown in Figure 6a are located in southern, not northern latitudes. This feature could be due to enhanced tropical wave activity associated with the occurrence of the tropical ENSO phenomenon, but there may also be global-scale effects, extending to low latitudes, from the SH final warming in late 1982. (The 1982 SH final warming is discussed in detail by *Mechoso et al.* [1988].)

Unlike eastward waves 1–2, westward waves 3–6 in Figure 6b show smallest values of cross spectra near the equator. Because of the series normalization used in this figure, this observation may be expected for westward propagating normal modes, ER or RG waves. In theory, for all of these modes, largest geopotential and zonal wind perturbations occur not along the equator but rather at higher latitudes in either the tropics or the extratropics; this may also be said for meridional wind perturbations, with the exception of RG waves in which these winds are largest along the equator. If waves 3–6 contribute to the westward acceleration phase of the QBO, the largest positive quadspectra (Figure 6b, bottom frame) observed near 10 hPa suggest that greatest amplitudes in TOMS waves 3–6 coincide with the westward acceleration of the QBO zonal winds at altitudes near or above the 10-hPa pressure level. (This can also be seen in Figure 2 for events W2–W5.) Furthermore, Figure 6b (bottom) shows a distinct 1/4 cycle phase lag, rather than phase lead, in both hemispheres around 40–50 hPa.

A reasonable conclusion from these results is that instead of strongest zonal waves 3–6 episodes directly affecting tropical QBO winds, the latter may instead tend to have a filtering effect on westward waves 3–6. These waves presumably have long vertical wavelengths and are comprised mostly of global normal modes and ER waves. If they have a role in forcing the westward acceleration of the QBO, it is most likely that this effect would be limited to altitudes near the upper levels of the QBO (roughly, around 5–10 hPa). This result may be compared with strongest westward events W2–W5 in Figure 3 which occur during dominant eastward winds throughout the lower stratosphere. However, as discussed in section 4.2, absorption of the weaker meridionally symmetric and antisymmetric waves 3–6 for events W1′–W5′ may provide part of the acceleration of the westward phase of the QBO zonal wind.

The actual forcing of the westward QBO zonal wind phase is not fully understood. For example, *Takahashi and Boville* [1992] used a three-dimensional mechanistic model that allowed wave-wave interactions and found, for the first time, QBO structure in a global circulation model. Their model showed the rapid descent of the

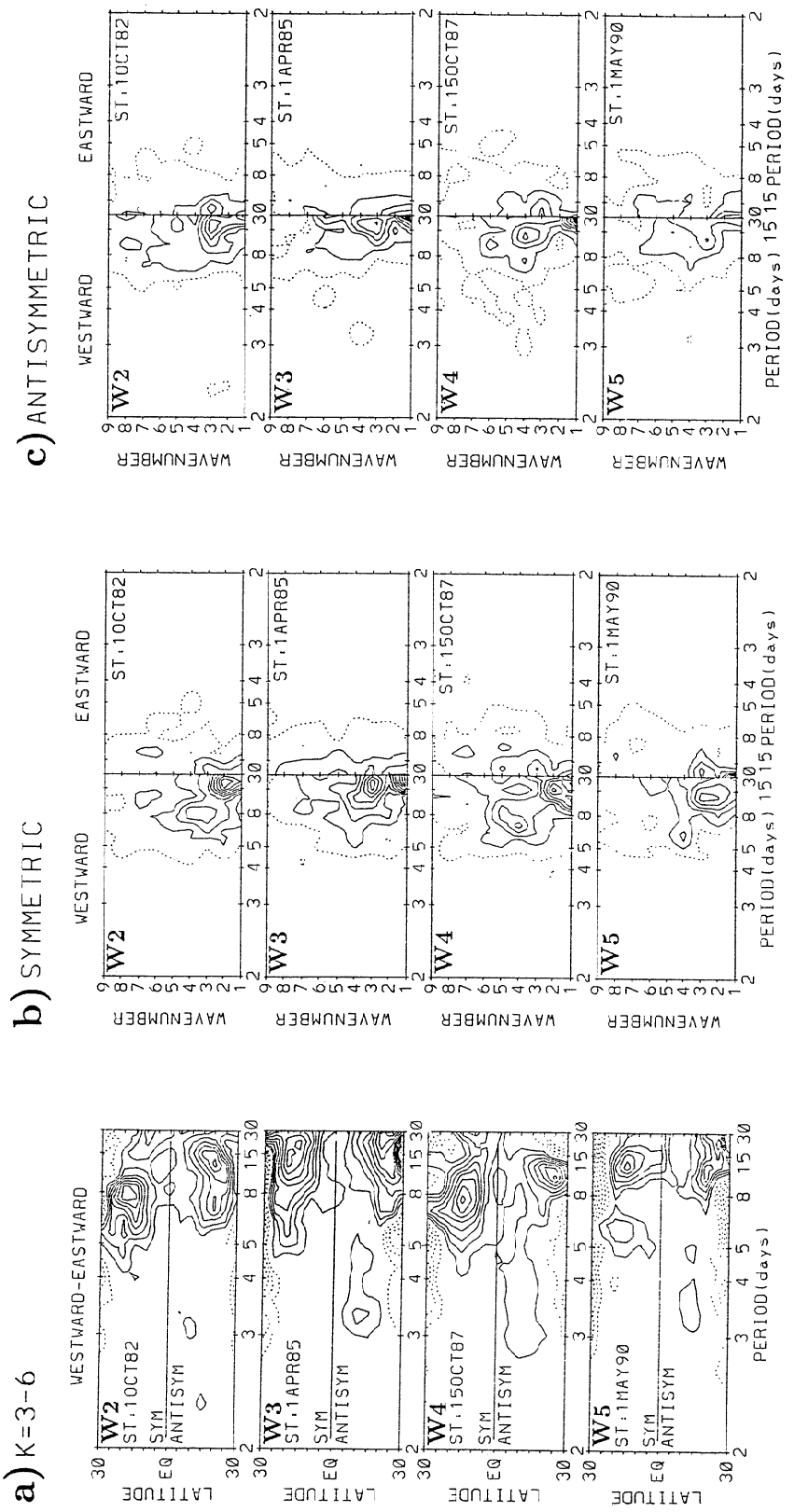

Figure 7. (a) Latitude versus frequency (periods in days indicated) plots of differential spectral amplitudes (westward minus eastward amplitudes) of meridionally symmetric and antisymmetric zonal waves 3–6 series for episodes W2-W5. The top (bottom) half of each frame is spectra calculated from meridionally symmetric (or antisymmetric) time series given by $[T(\phi)+T(-\phi)]/2$ (or $[T(\phi)-T(-\phi)]/2$), where ϕ is latitude and T denotes a TOMS time series. Each episode is 60 days long (starting date indicated in each frame). Dashed (solid) contours begin at -0.1 (0.1) and decrement (increment) by 0.1. Units are DU. (b) Zonal wavenumber versus frequency (periods in days shown) plots of meridionally symmetric and antisymmetric TOMS ozone spectral amplitudes for same 60-day episodes W2-W5. Dashed contours are 0.15. Solid contours begin at 0.3 and increment by 0.15. Units are DU. Spectra computed from meridionally symmetric time series given by $[T(20°\ N)+T(15°\ N)+T(15°\ S)+T(20°\ S)]/4$, where T is a TOMS time series. (c) Same as Figure 7b but calculations use meridionally antisymmetric series given by $[T(20°\ N)+T(15°\ N)-T(15°\ S)-T(20°\ S)]/4$.

eastward QBO phase, similar to observations. Their results also indicated that about two thirds of the eastward QBO forcing was due to Kelvin wave absorption, the rest being due to vertical advection of mean wind shear. Moreover, it was suggested that the theory of the QBO may be seriously deficient, with other momentum sources required for the forcing of the westward QBO phase, to augment the RG wave. Possible other sources include extratropical planetary waves [*Andrews and McIntyre*, 1976; *Dunkerton*, 1985] or gravity waves, as in the original *Lindzen and Holton* [1968] theory. The modeling studies by *Takahashi and Holton* [1991] suggested that Rossby waves are not the primary forcing mechanism. However, in retrospect, the dashed curve in Figure 3 for antisymmetric events W1′–W5′ does indeed show evidence of relative maxima during the westward transition phase of the QBO winds and may indicate at least partial forcing of this QBO phase.

6.2. Strongest Westward Episodes

Meridional symmetries and antisymmetries for the strongest westward events, W2–W5, are shown in Figure 7a. (Note that the top and bottom of each of the four panels correspond to symmetric and antisymmetric components, respectively.) A plotting scheme is used in which eastward spectral amplitudes were subtracted from westward amplitudes at each frequency and latitude to highlight dominant westward phase propagation and tropical confinement of these events. A useful result from Figure 7a is a direct examination of the meridional distributions of symmetric and antisymmetric waves 3–6. Largest amplitudes in meridionally symmetric components consistently maximize around latitudes 15°–20°with oscillation periods ~7–15 days. On the other hand, amplitudes for meridionally asymmetric components maximize around 20°–25°for lower frequencies (conceivably including ER modes), but for shorter periods ~3–6 days (including RG waves) they appear to maximize in lower latitudes around 10°–15°.

Meridionally symmetric and antisymmetric spectral amplitudes of episodes W2–W5 for zonal wavenumbers 1–9 are shown in Figure 7b and 7c, respectively. Three of the most mode-selective cases appear to be in the symmetric components (Figure 7b) for episodes W2 (wave 2), W4 (mixed waves 2 and 4), and W5 (waves 2 and 3).

We first examine the 1982 episode W2, in which Figure 7b shows a symmetric westward propagating zonal wave 2 in TOMS. Episode W2 also indicates a mode in asymmetric wave 3, but subsequent 8 to 30-day bandpass data (figures not shown) show that this asymmetric wave 3 event occurs around 15 days before the symmetric wave 2 event; the primary mode over the 60-day segment beginning October 15, 1982 is still the symmetric wave 2 where peak amplitudes (~5 DU) are approximately double those found in asymmetric wave 3. For event W2 there is a distinct similarity between total ozone and 10-hPa geopotential heights, as demonstrated in Figure 8a which shows a clear westward prop-

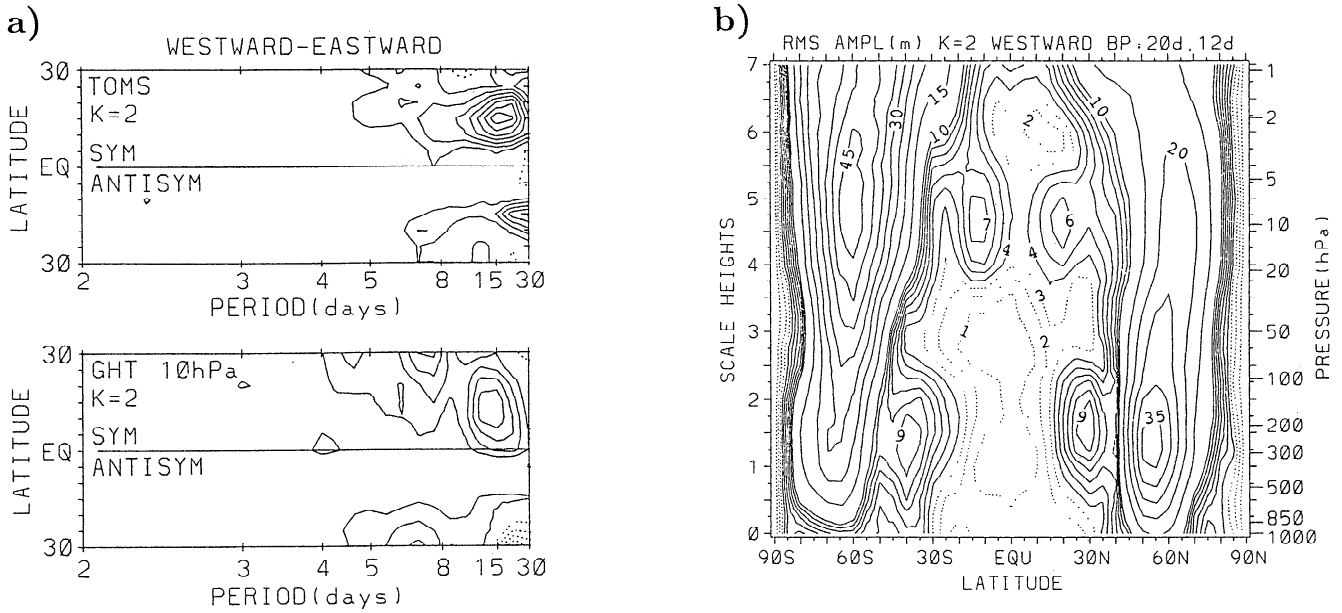

Figure 8. (a) Latitude versus frequency (periods in days indicated) zonal wave 2 meridionally symmetric/antisymmetric spectral amplitudes of (top) TOMS ozone and (bottom) 10-hPa geopotential heights. (See Figure 7a caption for symmetric/antisymmetric plotting definitions.) Time series are 60 days long, beginning September 15, 1982. For TOMS ozone, dashed (solid) contours begin at -0.15 (0.15), decrementing (incrementing) by 0.15; units are DU. For 10-hPa geopotential heights, dashed (solid) contours begin at -1 (1) and decrement (increment) by 1; units are meters. (b) Corresponding 60-day log-pressure scale height versus latitude cross section of computed rms amplitudes of westward zonal wave 2 band-pass filtered geopotential heights. Band-pass filter (half-amplitude response at periods 20 and 12 days) highlight primary geopotential height wave 2 frequency response in Figure 8a. Dashed contours are 1, 2, 3. Solid contours are 4, 5, ..., 9 and in higher latitudes 10, 15, 20, ... Units are meters.

agating, meridionally symmetric wave with maximum amplitude around latitude 15° and period ~15 days for both of these independent data sets. (Figure 8a has a slightly different starting date than Figure 7b, to emphasize wave 2 features.)

Root-mean-square amplitudes of westward zonal wave 2 band-pass filtered geopotential height series were given in Figure 8b to further investigate the 10-hPa wave 2 in Figure 8a. Figure 8b shows several features, including relative maxima near 200 hPa at latitudes 30°N and 40°S which is similar in structure to a westward propagating (2,3) tropospheric normal mode. This particular 200-hPa disturbance was found to have little impact on tropical total ozone and was not investigated further in this study. A common notation for normal modes is $(n, m-n)$, where n denotes zonal wavenumber and m is a meridional wavenumber index. (Normal modes are discussed, for example, by *Salby* [1984] and *Venne* [1989].) Studies by *Salby* [1984] and *Venne* [1989] provide examples of this mode but do not show evidence for such low-latitude confinement in the stratosphere. Time series for this wave 2 event in TOMS (dark curves) and 10-hPa geopotential heights (light) are shown in Figure 9; note that the two data sets exhibit a moderate amount of temporal similarity. This wave 2 feature might best be described as an ER wave in the stratosphere since it appears equatorially trapped. Examination of the vertical structure for this wave 2 event in geopotential heights indicates long vertical wavelengths exceeding four scale heights, but because stratospheric height data were derived using SSU temperatures with coarse vertical weighting functions (each spanning ~2–3 scale heights), determination of vertical wavelengths and amplitudes is difficult.

Hovmöller (time versus longitude) diagrams of meridionally symmetric TOMS waves 3–6 and wave 2 are shown in Figure 10. Two strong events appear in waves 3–6, one in October and the other in November 1987.

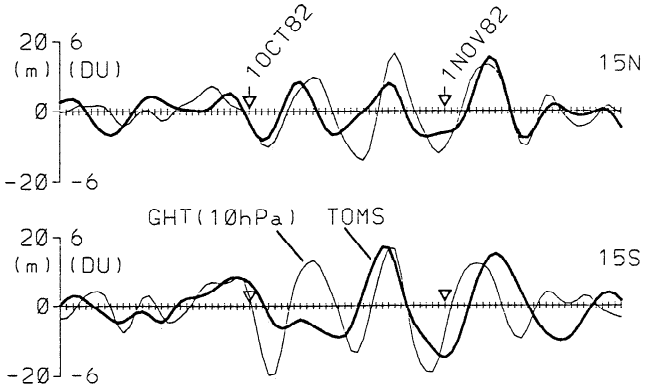

Figure 9. Time series of zonal wave 2 band-pass filtered (half-amplitude response at 30- and 5-day periods) TOMS ozone (dark) and 10-hPa geopotential heights (light) at latitudes 15°N and 15°S and longitude 180°. Dates, 60 days, starting September 15, 1982. One day per tick mark. Vertical axes denote linear plotting scales for TOMS ozone (geopotential height) perturbations in units DU (meters).

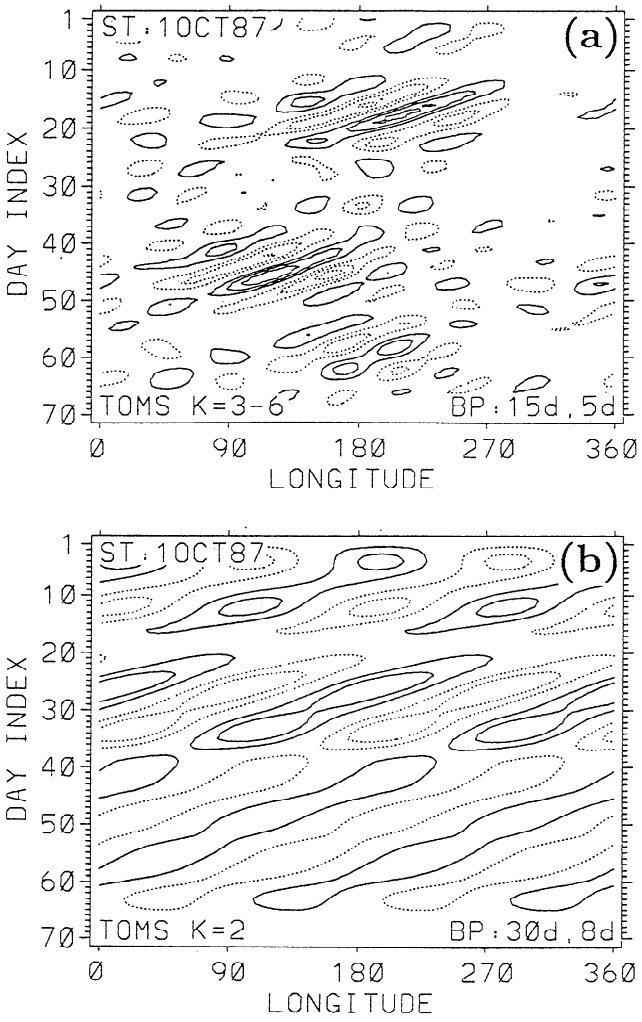

Figure 10. Hovmöller diagrams for (a) symmetric TOMS zonal waves 3–6 and (b) wave 2 derived by averaging time series at 15°N and 15°S. No eastward/westward filtering. Starting date is October 1, 1987. In Figure 10a, solid (dashed) contours begin at 2 (-2) and increment (decrement) by 2; for Figure 10b solid (dashed) contours begin at 1 (-1) and increment (decrement) by 1. Units are DU. Band-pass filters were used to capture observed primary spectral responses. (Half-amplitude response periods are shown in each frame.)

The November event corresponds to episode W4 (60 days beginning October 15) in Figure 7. Maximum amplitudes in waves 3–6 for both events exceed 6 DU, double the corresponding wave 2 amplitudes which are ~1–3 DU. Note that the waves 3–6 episodes show evidence of westward phase propagation and eastward wavepacket group velocity. Based on its latitudinal symmetry and localized confinement along longitude, event W4 in waves 3–6 is tentatively attributed to a meridionally symmetric mixed ER wave. It is less likely that this disturbance is a mixed RG wave since RG waves in total ozone might generally be expected to exhibit meridional asymmetry (see section 3 and Figure 1) with largest amplitudes located closer toward the equator (~5°–10°). However, as noted in SZ, the asymmetry

characteristic may be altered by meridional gradients in mean ozone.

Event W5 appears to be dominated by a meridionally symmetric zonal wave 3 with period ~13 days (see Figure 7) and is similar to a (3,3) global normal mode. *Venne* [1989] examined several climatological global normal modes, including a meridionally symmetric wave 3 with period ~15 days, denoted as a (3,3) normal mode. Analyses in the present study (figures not shown) of wave 3 geopotential height data indicated peak disturbance amplitudes in the vertical around 7 hPa, with meridional symmetry throughout the tropics; maximum amplitudes of pure westward components in both data series occurred near latitudes 25°–30°S. Time series of zonal wave 3 band-pass TOMS ozone and 7-hPa geopotential heights are shown in Figure 11. Meridional symmetry and general positive cross correlation are both apparent in this figure. Peak amplitudes in TOMS are ~3–5 DU. Because of the episodic nature, quantitative correlation calculations were not performed.

In conclusion, strongest westward propagating wave events exhibit characteristics which are consistent with both tropical ER waves and global normal modes. For these episodes, TOMS and middle stratosphere geopotential height data show similar wave propagation characteristics.

6.3. Secondary Westward Episodes

As noted in section 4.2, during the westward transition phase of the QBO, both meridionally symmetric and asymmetric westward components in TOMS data show evidence of enhanced wave activity. Of the five secondary episodes W1′–W5′ (see Figure 3) examined over lengthy (~180 days) segments, W1′, W3′, and W4′ were found to provide the clearest evidence of tropical wave modes. Figures 12a and 12b show space-time spectra for these three events. Since these cases were found to be highly episodic with ~10 to 15-day lifetimes, a 20-day window centered about each episode was used in calculating spectra. Figure 12a indicates that all three events exhibit a distinct westward propagation of symmetric components with periods around 4–7 days. More surprising, W3′ also shows asymmetric RG wave signatures in wave 4 with a period around 4–5 days. Because it is unique to find RG waves in total ozone, asymmetric components for W3′ are examined in the following parts of Figure 12.

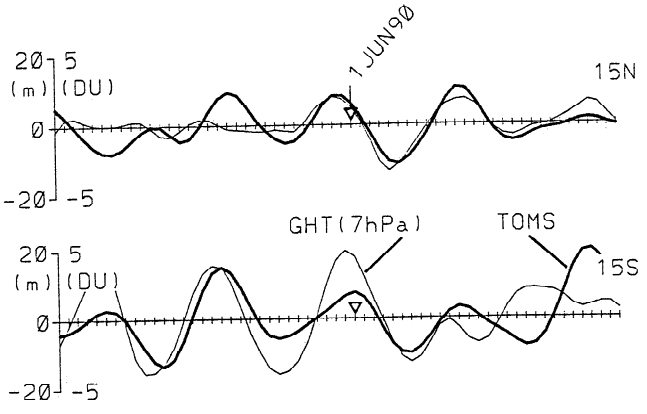

Figure 11. Same as Figure 9 but for zonal wave 3 with starting date May 1, 1990.

Band-pass time-longitude plots for these same three events are shown in Figures 12c-12d. Westward phase and eastward wave packet propagation are evident in each case in Figure 12c. (Eastward group velocities are distinguishable by following centroids of peak perturbation amplitudes that are seen to propagate eastward with time.) Signatures for event W3′ depict an RG wave induced east of the dateline. Initiation of episodes W1′ and W4′ appear to be related to westward propagation of longer-scale waves. For these two cases, Figure 12d indicates that lower wavenumber disturbances propagate westward with approximately the same phase speed in days immediately before and during the onset of the higher wave modes shown in Figure 12c.

The study by *Dunkerton* [1993] examined nearly 20 years of rawinsonde data from several tropical western Pacific stations and classified four general types of oscillations with time periods 3–6 days. Most dominant was a wave 4–6 RG structure with largest amplitudes around 250 hPa near the dateline with periods slightly greater than 5 days. A second type was lower-tropospheric broadband activity located in the western Pacific during NH summer. A third kind was an oscillation with period ~$4\frac{1}{2}$ days which exhibited largest amplitudes in the lower troposphere and occurred in the central Pacific during NH autumn. The fourth type classified was stratospheric RG waves 3–4 with periods ~4 days; these oscillations were largest during the eastward phase of the QBO in the lower stratosphere. In Figure 12c, events W1′ and W4′ indicate an origin in the western Indian Ocean region, which lies outside the zonal regions analyzed by *Dunkerton* [1993]. In comparison, event W3′ appears to originate in the east central Pacific and exhibits features consistent with RG wave dynamics in total ozone; such features include a lower-latitude confinement and meridional asymmetry. If tropospheric convection were the source for these modes, then the excitation regions deduced from TOMS might not reflect true excitation regions because there could be a considerable longitudinal shift as disturbances propagate vertically upward into the stratosphere where most ozone exists. As an example, the tropical model by *Holton and Lindzen* [1972] for a 5-day tropospheric heat source which was antisymmetric about the equator showed ~180° longitudinal eastward shift of meridional wind perturbations from 10 to 25 km altitudes in the presence of lower-stratospheric eastward winds. (This particular model indicated a zonal wave 4 RG wave as the dominant mode.)

Examination of BMO geopotential data for episodes W1′–W5′ provide only marginal clues to their origin. For W1′ and W3′ in Figure 12 the BMO data are incoherent with TOMS. This would not be unexpected for event W3′ if it indeed is a RG wave where vertical wavelengths may be too short to be detected in BMO data. For W4′, BMO data indicate (figures not shown) a westward 4 to 5-day meridionally symmetric ER wave 4 in the tropics near the tropopause that also coincides

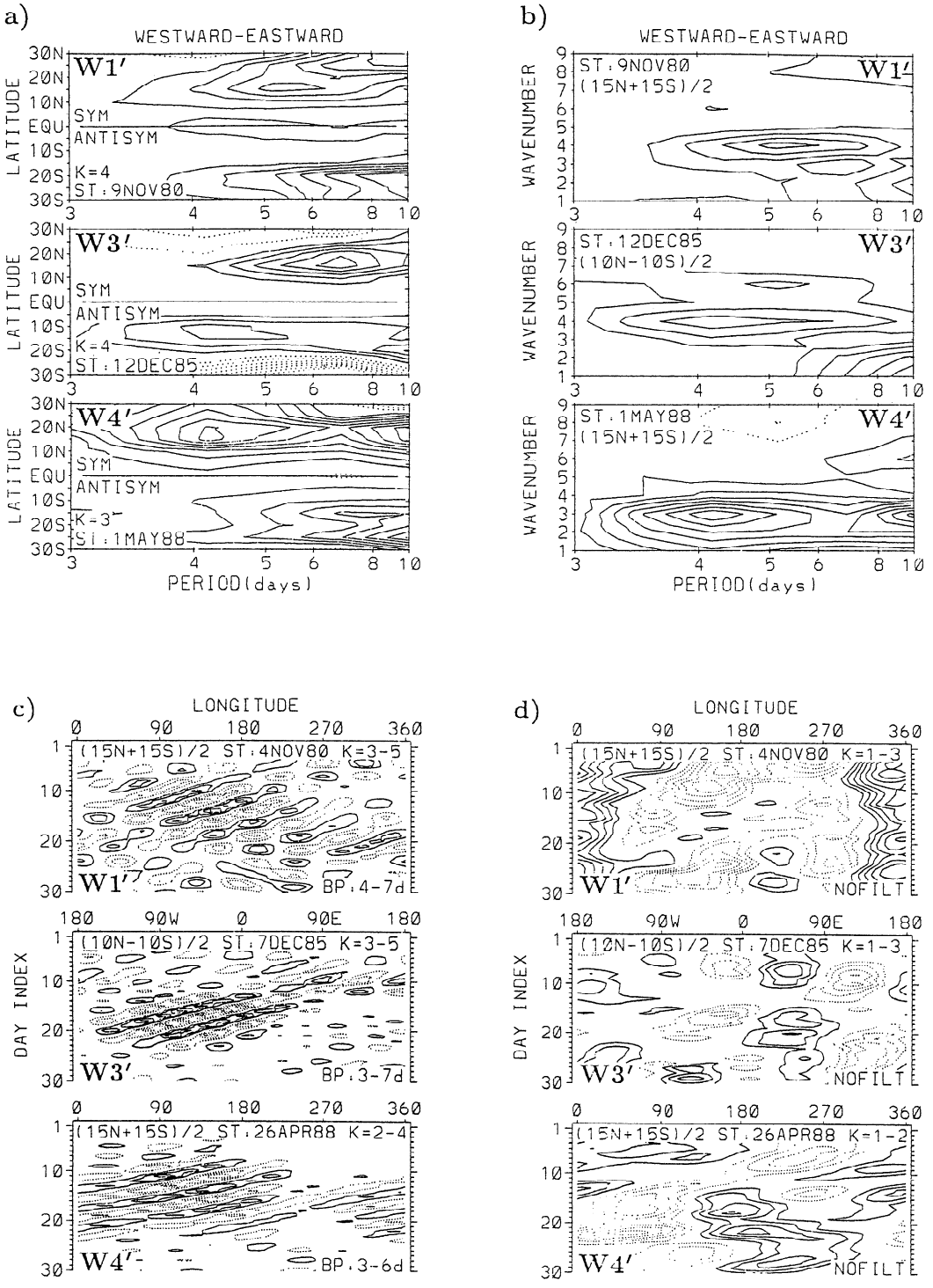

Figure 12. (a–b) Spectral amplitudes for 20-day segments with starting dates indicated. Units are DU. Dashed (solid) contours begin at -0.1 (0.1) and decrement (increment) by 0.1. (a) Top (bottom) are meridionally symmetric (asymmetric) westward minus eastward amplitudes (fixed zonal wavenumbers shown). (b) Zonal wavenumber versus frequency spectral amplitudes with meridional symmetries indicated. (c–d) Time versus longitude with combined eastward and westward components. Meridional symmetries indicated. Units are DU. (c) Half-amplitude band-pass time periods indicated in each frame. Dashed (solid) contours begin at -0.5 (0.5) and decrement (increment) by 0.5 for events W1′ and W3′. For W4′ dashed (solid) contours begin at -1 (1) and decrement (increment) by 1. (d) Lower wavenumbers (indicated in each frame) and no temporal filtering. Dashed (solid) contours begin at -1.5 (1.5) and decrement (increment) by 1.5.

with an apparent westward 4-day symmetric ER wave 4 in the middle stratosphere subtropics around 5 hPa; the latter wave maximizes around 20°–30°in both hemispheres.

In short, the secondary wave episodes (W1′–W5′) in TOMS ozone occur when tropical QBO zonal winds change from eastward to westward directions in the middle stratosphere. Because vertically integrated ozone (total ozone) tends to smooth out signals of tropical waves, these events show only sporadic evidence of distinct space-time modes (for example, W1′, W3′, and W4′ in Figure 12). It is conceivable that either convection or wave-wave interaction is responsible for excitation of these episodes (beyond the scope of this study). Clearest cases indicate both ER and RG waves.

7. Summary

This study provides a detailed investigation of a previously discovered synchronization between the tropical QBO winds and episodes of fast tropical waves in TOMS total ozone. Largest TOMS wave amplitudes are observed when their direction of propagation is primarily opposite those of tropical (Singapore) QBO zonal winds (particularly around 30 hPa). Analyses of waves 1-2 and 3–6 for periods shorter than 15 days indicate greatest variance in the meridionally symmetric modes. These analyses, including QBO cross-spectra calculations between Singapore lower-stratospheric winds and eastward waves 1–2 in TOMS, show evidence of Kelvin waves during the descending eastward transition phase of the QBO zonal winds, consistent with downward propagation of the absorption level for Kelvin waves and forcing of this QBO phase.

Analyses of westward waves 3–6 in TOMS are consistent with possible forcing of the westward QBO wind phase by episodes of both meridionally symmetric and asymmetric westward waves (W' events in the text); space-time analyses show that both ER and RG waves are discerned in these episodes. In contrast to the case of eastward (Kelvin) waves the strongest westward events (W events in the text) appear to be filtered by, rather than forcing, the westward phase of the stratospheric QBO wind. These dominant westward episodes are interpreted as meridionally symmetric westward global normal modes and tropically confined ER waves 2–6. The events exhibit phase and group speeds characteristic of wave dynamics rather than simple wind advection.

Acknowledgments. We thank Patricia T. Guimaraes, Richard D. McPeters, Arlin J. Krueger, and the members of the NASA TOMS Nimbus Experiment and Information Processing Teams, and the National Space Science Data Center for providing the TOMS data on CD-ROM disk. We also thank the British Meteorological Office for supplying the geopotential height data used in this study. This work was supported by National Aeronautics and Space Administration grant NAG 5–1519.

References

Andrews, D. G., and M. E. McIntyre, Planetary waves in horizontal and vertical shear: The generalized Eliassen-Palm relation and the mean zonal acceleration, *J. Atmos. Sci., 33*, 2031–2048, 1976.

Andrews, D. G., J. R. Holton, and C. B. Leovy, *Middle Atmosphere Dynamics*, 489 pp., Academic, San Diego, Calif., 1987.

Bowman, K. P., Evolution of the total ozone field during the breakdown of the Antarctic circumpolar vortex, *J. Geophys. Res., 95*, 16,529–16,543, 1990.

Dunkerton, T. J., A two-dimensional model of the quasi-biennial oscillation, *J. Atmos. Sci., 42*, 1151–1160, 1985.

Dunkerton, T. J., Observation of 3-6 day meridional wind oscillations over the tropical Pacific 1978–1992: Vertical structure and interannual variability, *J. Atmos. Sci., 50*, 3292–3307, 1993.

Holton, J. R., and R. S. Lindzen, An updated theory for the quasi-biennial cycle of the tropical stratosphere, *J. Atmos. Sci., 29*, 1076–1080, 1972.

Lindzen, R. S., and J. R. Holton, A theory of the quasi-biennial oscillation, *J. Atmos. Sci., 25*, 1095–1107, 1968.

Maruyama, T., Annual and QBO-synchronized variations of lower-stratospheric equatorial wave activity over Singapore during 1961–1989, *J. Meteorol. Soc. Jpn., 69*, 219–232, 1991.

McCormick, M. P., and M. T. Osborn, Airborne lidar measurements of El Chichon stratospheric aerosols, *NASA Ref. Publ. 1136.*, 1985.

Mechoso, C. R., A. O'Neill, V. D. Pope, and J. D. Farrara, A study of the stratospheric final warming of 1982 in the southern hemisphere, *Q. J. R. Meteorol. Soc., 114*, 1365–1384, 1988.

Murakami, M., Large-scale aspects of deep convective activity over the GATE area, *Mon. Weather Rev., 107*, 994–1013, 1979.

Randel, W. J., Upper tropospheric equatorial waves in ECMWF analyses, *Q. J. R. Meteorol. Soc., 118*, 365–394, 1992.

Salby, M. L., Survey of planetary-scale waves: The state of theory and observations, *Rev. Geophys., 22*, 209–236, 1984.

Shiotani, M., Annual, quasi-biennial, and El Niño-Southern Oscillation (ENSO) timescale variations in equatorial total ozone, *J. Geophys. Res., 97*, 7625–7633, 1992.

Shiotani, M., and T. Horinouchi, Kelvin wave activity and the quasi-biennial oscillation in the equatorial lower stratosphere, *J. Meteorol. Soc. Jpn., 71*, 175–182, 1993.

Stanford, J. L., and J. R. Ziemke, Rossby-gravity waves in tropical total ozone, *Geophys. Res. Lett., 20*, 2239–2242, 1993.

Takahashi, M., and B. A. Boville, A three-dimensional simulation of the equatorial quasi-biennial oscillation, *J. Atmos. Sci., 49*, 1020–1035, 1992.

Takahashi, M., and J. R. Holton, The mean zonal flow response to Rossby waves and gravity wave forcing in the equatorial lower stratosphere: Relationship to the QBO, *J. Atmos. Sci., 48*, 2078–2087, 1991.

Thompson, A. M., D. P. McNamara, K. E. Pickering, and R. D. McPeters, Effect of marine stratocumulus on TOMS ozone, *J. Geophys. Res., 98*, 23,051–23,057, 1993.

Venne, D. E., Normal-mode Rossby waves observed in the wavenumber 1–2 geopotential fields of the stratosphere and troposphere, *J. Atmos. Sci., 46*, 1042–1056, 1989.

Ziemke, J. R., and J. L. Stanford, One-to-two month oscillations in the stratosphere during Southern winter, *J. Atmos. Sci., 47*, 1778–1793, 1990.

Ziemke, J. R., and J. L. Stanford, Kelvin waves in total column ozone, *Geophys. Res. Lett., 21*, 105–108, 1994.

J. L. Stanford and J. R. Ziemke, Department of Physics and Astronomy, Iowa State University, Ames, IA 50011.

(Received February 8, 1994; revised August 11, 1994; accepted August 15, 1994.)